Magnetocaloric effect and critical behavior of the Mn-rich itinerant material Mn_3GaC with enhanced ferromagnetic interaction*

Pengfei Liu(刘鹏飞)[1,2], Jie Peng(彭杰)[1], Mianqi Xue(薛面起)[2], and Bosen Wang(王铂森)[3,†]

[1] *Hunan Key Laboratory for Micro-Nano Energy Materials and Devices and School of Physics and Optoelectronics, Xiangtan University, Xiangtan* 411105, *China*

[2] *Technical Institute of Physics and Chemistry, Chinese Academy of Sciences, Beijing* 100190, *China*

[3] *Beijing National Laboratory for Condensed Matter Physics and Institute of Physics, Chinese Academy of Sciences, Beijing* 100190, *China*

(Received 19 January 2020; revised manuscript received 2 March 2020; accepted manuscript online 9 March 2020)

We revisit the reversible magnetocaloric effect of itinerant ferromagnet Mn_3GaC near the ferromagnetic to paramagnetic phase transition by adopting the experimental and theoretical methods and critical behavior of Mn-rich Mn_3GaC with an enhanced FM interaction. Landau theory model cannot account for temperature dependent magnetic entropy change which is estimated from thermal magnetic methods only considering magnetoelastic coupling and the electron–electron interaction, apart from molecular mean-field model. Critical behavior is studied by adopting the modified Arrott plot, Kouvel–Fisher plot, and critical isotherm analysis. With these critical exponents, experimental data below and above T_c collapse into two universal branches, fulfilling the single scaling equation $m = f_{\pm}(h)$, where m and h are renormalized magnetization and field. Critical exponents are confirmed by Widom scaling law and just between mean-field model and three-dimensional Heisenberg model, as the evidence for the existence of long-range ferromagnetic interaction. With increasing the Mn content, T_c increases monotonously and critical exponents increases accordingly. The exchange distance changes from $J(r) \sim r^{-4.68}$ for $x = 0$ to $J(r) \sim r^{-4.71}$ for $x = 0.08$, respectively, which suggests the competition of the Mn–Mn direct interaction and the itinerant Mn–C–Mn hybridization. The possible mechanism is proposed.

Keywords: magnetocaloric effect, critical behavior, Mn_3GaC

PACS: 75.20.En, 75.30.Sg, 75.60.Ej **DOI:** 10.1088/1674-1056/ab7da1

1. Introduction

Itinerant electronic materials are excellent candidates to explore functional materials. Among them, Mn-based itinerant materials are such examples that have attracted more attention due to the important findings including giant magnetoresistance (GMR),[1,2] magnetocaloric effect (MCE),[3–6] negative thermal expansion (NTE),[7–13] and magnetostriction (MS),[14–16] *etc.* Mn_3GaC exhibits various magnetic/structural phase transitions and has been widely investigated.[1–5,17–19] With decreasing temperature, it transits from paramagnetic (PM) to ferromagnetic (FM) phases at 250 K, to an intermediate canted ferromagnetic (IFM) phase at 158 K, and to an antiferromagnetic ground state with discontinuous expansion in lattice parameter near 155 K.[17,19] Accompanied by magnetic/structural phase transitions, GMR can reach nearly 80% at 5 T and larger "trapeziform"-like negative magnetic entropy changes exists.[1–5] Meanwhile, giant isotropic MS (1700 ppm) is found near the AFM–IFM phase transition.[15] In addition to important experimental findings, some basic scientific issues remain controversial on these FM materials after many years of exploration.

The first controversial point is Mn–Mn interaction of this system although different models have been proposed, such as the Ruderman–Kittel–Kasuya–Yosida (RKKY) interaction, the direct-coupling model, and the mean field models. No systematic and in-depth theoretical calculations were performed to reveal the internal mechanism of magnetic interactions although similar tries were carried out in other itinerant FM materials. Another point is why FM–PM transition is so sensitive to Mn-doping only considering lattice changes. In other words, its Fermi surface structure nesting and energy band filling effect can play a key role. For Mn-rich Mn_3GaC, a reversible MCE with large temperature spans at T_c is reported,[20] while the origin of quickly enhanced T_c with Mn-doping and the studies of MCE based on various theoretical models are lacking. Previous investigations have proved that critical exponent analysis in the vicinity of magnetic transition is a powerful to single out the relevant microscopic interaction.[21–27] According to the reports,[17,20] Mn_3GaC is an itinerant electronic material and electron-electron interaction is important to carrier transporting and mainly comes from Mn-3d band electrons. Its ground state can be well-described by Fermi-liquid behavior. Meanwhile, electron-phonon interaction may be important in contributing magnetic entropy change near phase transitions. In this respect, more theoretical and experimental investigations are required to deepen our understanding of magnetic properties of this system.[21,22] In this work, we present a detailed study on

*Project supported by National Key Research and Development Program of China (Grant Nos. 2018YFA0305700 and 2018YFA0305800), One Hundred-Talent Program in Institute of Physics (Grant No. Y7K5031X61), Youth Promotion Association of CAS (Grant No. 2018010).

†Corresponding author. E-mail: bswang@iphy.ac.cn

the MCE near the FM–PM transition based on Landau theory of the transition model and the molecular mean-field model and on the specific heat. We find that the simple Landau theory model can not account for the temperature dependence of magnetic entropy in Mn_3GaC if only considering magnetoelastic coupling and electron-electron interaction. The scaling plots confirm that critical exponents are reliable and all the critical exponents are just between the mean-field model and the three-dimensional (3D) Heisenberg model, as the evidence for the existence of long-range FM interaction. The exchange distance changes from $J(r) \sim r^{-4.68}$ for $x = 0$ to $r^{-4.71}$ for $x = 0.08$, respectively, which suggests the competition of Mn–Mn direct interaction (180°) and the itinerant Mn–C–Mn (90°) hybridization.

2. Experimental details

Polycrystalline samples Mn-rich Mn_3GaC was prepared as reported previously,[1,2] and structural parameters were collected by x-ray diffraction (Cu $K\alpha$, $\lambda = 0.15406$ nm). Magnetic properties were measured on a Quantum Design superconducting quantum interference device magnetometer (1.8 K $\leq T \leq$ 400 K, $0 \leq H \leq$ 50 kOe). The sample for magnetic measurements can be considered as ellipsoids and the applied field is parallel to its longest semiaxis. Thus, a uniform field exists throughout the sample and sharp demagnetizing fields could be reduced. Thermopower coefficient was measured by using standard four-probe technique in the Quantum Design physical property measurement system (1.8 K $\leq T \leq$ 400 K, $0 \leq H \leq$ 90 kOe). The Rietveld refinement of XRD pattern indicates that all the samples are single-phase (SG: $Pm\bar{3}m$) with lower R_p and R_{wp}. Refined lattice constant of Mn_3GaC is about 0.3897(3) nm, close to the reported value (0.3896 nm).[1,3,17] With increasing the substitution of Ga by the excess Mn, the lattice parameter decreases linearly.

3. Results and discussion

3.1. Direct-current magnetization

Figure 1 shows the temperature dependence of $M(T)$ curves for $Mn_{3+x}Ga_{1-x}C$ under the zero-field-cooled (ZFC) process. In Fig. 1(a), $M(T)$ is measured at different fields for Mn_3GaC under the ZFC process and the temperature dependence of dM/dT is used to search the corresponding transition temperature. The inset describes magnetic structures of the FM phase. We find that its peak temperature shifts to higher temperature with increasing the field from 0.1 kOe to 10 kOe, which indicates enhanced FM interaction at higher fields.[1,17] Inverse susceptibility is plotted and well-described by the modified Curie–Weiss law: $\chi(T) = C/(T-\theta) + \chi_0(1+AT^2)$, where the first term $C/(T-\theta)$ represents the Curie–Weiss contribution, the second term $\chi_0(1+AT^2)$ is the Pauli PM contribution from enhanced exchanges with the $\chi_0 AT^2$ being the modified term, and A reflects electronic energy state shape at the Fermi level. In an external field, a small amount of energy is transmitted near the Fermi surface owing to different energies between spin-up and spin-down conduction electrons: $\chi_0 = 3.56(8)$ emu·K/mol, $A = -2.99(4) \times 10^{-6}$ emu/(mol·K^2). Effective moment is given by $\mu_{eff} = 2.83(C/\eta)^{0.5}\mu_B = 3.086\mu_B$, where η is the number of magnetic atoms in a unit cell. Similarly, both the $M(T)$ and dM/dT of $Mn_{3+x}Ga_{1-x}C$ are shown in Fig. 1(b). We find that, with the increase of Mn-doping content, the peak height decreases and the peak width increases, and it T_c shifts to high temperature. The derivatives are found to be 250 K, 281.5 K, 296.5 K, and 323.5 K for $x = 0$, 0.06, 0.07, and 0.08, respectively. The enhancement of the T_c can be attributed to lattice contraction, which leads to an enhanced FM exchange interactions. However, this enhancement cannot be explained if ignoring band filling as a function of Mn-doping according to the compressibility of Mn_3GaC under pressure. In this work, we discuss the MCE by experimental/theoretical methods and the critical behaviors of Mn-rich Mn_3GaC based on the thermo-dynamical theory.[20] Different theoretical models are adopted to quantify entropy change of this system, such as the Landau theory model and the mean-field model.[28–32]

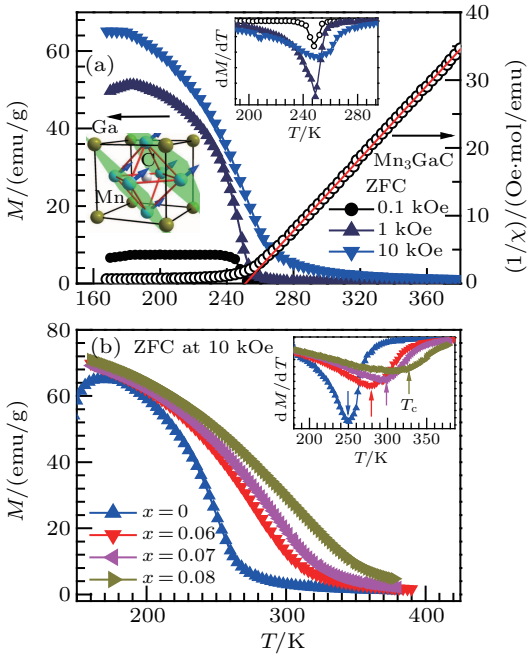

Fig. 1. (a) Temperature dependent $M(T)$ in zero-field-cooled (ZFC) process. Inset: magnetic structures and dM/dT. Inverse susceptibility on the right of Fig. 2(a); (b) $M(T)$ for $Mn_{3+x}Ga_{1-x}C$ at 1 T.

3.2. The MCE — Landau theory model

In Fig. 2(a), $M(H)$ data are plotted for Mn_3GaC (192–288 K) Arrott plots derived from $M(H)$ covering a broad temperature. The Gibbs free energy G is expressed as

$$G(T,M) = G_0 + \frac{1}{2}AM^2 + \frac{1}{4}BM^4 - MH, \quad (1)$$

where A and B are the temperature-dependent parameters containing the magneto-elastic coupling and the electron interaction. From the equilibrium condition $\partial G/\partial M = 0$, the magnetic equation of state is

$$H/M = A + BM^2. \tag{2}$$

The H/M vs. M^2 plot has positive slopes, indicating second-order transition by Banerjee criterion.[33] From the differential Gibbs free energy, magnetic entropy is

$$S_{\mathrm{M}}(T,H) = -\frac{1}{2}\frac{\partial A}{\partial T}M^2 - \frac{1}{4}\frac{\partial B}{\partial T}M^4. \tag{3}$$

The temperature dependences of A and B are obtained by linear fitting (Fig. 2(b)). It is found that A varies from negative to positive with increasing the temperature, and the temperature is corresponding to $A = 0$ and is basically consistent with the T_{c}. As shown in Fig. 2(c), B keeps positive and is the feature of ferromagnic materials.[28,34] As we know, A can describe the electron interaction part of Gibbs free energy, and B represents the magneto-elastic part, which plays an important role in determining entropy changes $-\Delta S_{\mathrm{M}}$.[29,35] From Eq. (3), $-\Delta S_{\mathrm{M}}$ is calculated with different ΔH.

Figure 2(d) displays the calculated and experimental $-\Delta S_{\mathrm{M}}$. We find that $-\Delta S_{\mathrm{M}}$ from Eq. (3) is about four times larger than the experimental value and the peak is 35 K lower. Theoretical/experimental results are of great discrepancy, which is mainly originated from the degradation linearity in the H/M vs. M^2 plot below T_{c}. This is related to the sign change of thermopower coefficient $S(T)$ as indicated in the previous investigations.[28,36] In inset of Fig. 2(b), temperature dependence of $S(T)$ for Mn_3GaC has two characteristics: a slope change of $S(T)$ exists at 250 K closely associated with the FM–PM transition; its sign changes from negative to positive around 215 K, matching with the peak of calculated $-\Delta S_{\mathrm{M}}$. Lastly, we may conclude that larger differences between the experimental and theoretical entropy changes are attributed to some ignored and critical factors such as the phonon-electron interaction.

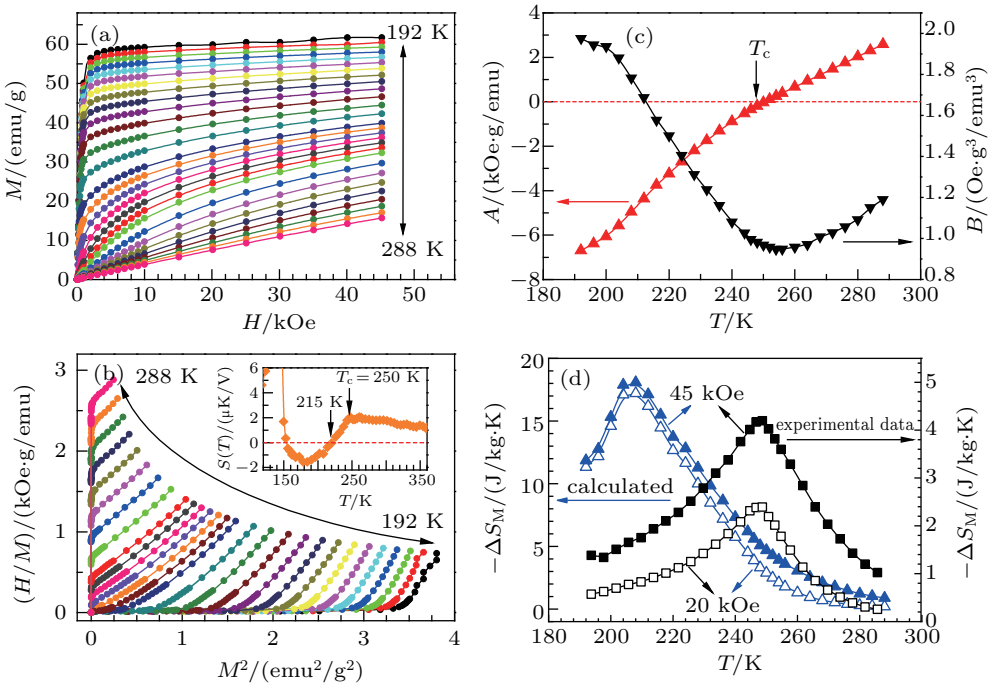

Fig. 2. (a) Isothermal magnetization curves $M(H)$; (b) Arrott plots derived from $M(H)$. Inset: temperature-dependent thermopower coefficient. (c) A (on the left) and B (on the right), where A and B are magneto-elastic coupling part and electron interaction part of the Gibbs free energy, respectively. (d) The calculated and experimental ΔS_{M} under $\Delta H = 20$ kOe and 45 kOe, respectively.

3.3. The MCE — mean-field scaling method

Another approach was adopted to apply the mean-field scenario to isothermal curves and calculate entropy changes.[31,32] It does not depend on the numerical integration of Maxwell relation and is a complementary approach to Landau theory.[29,31] Magnetic equation of state is expressed as

$$M(H,T) = f[(H + H_{\mathrm{exch}})/T], \quad H_{\mathrm{exch}} = \lambda M, \tag{4}$$

where f is the mean-field state function, H_{exch} is the exchange field, and λ is the exchange parameter. Generally, H_{exch} could be obtained by a series of odd powers of M. In this work, H_{exch} is taken as $H_{\mathrm{exch}} = \lambda_1 M + \lambda_3 M^3$, where λ_3 describes the magneto-volume effects as the Bean and Rodbell formulation.[37] The inverse $f^{-1}(M)$ function is

$$\frac{H}{T} = f^{-1}(M) - \frac{H_{\mathrm{exch}}}{T}, \quad \text{or} \quad \frac{H}{MT} = \frac{f^{-1}(M)}{M} - \frac{1}{T} \times \frac{H_{\mathrm{exch}}}{M}. \tag{5}$$

For a constant M, the $H_{\rm exch}$, $f^{-1}(M)$, and $f^{-1}(M)/M$ are constant if $H_{\rm exch}$ only depends on M. Accordingly, the plots of H/T vs. $1/T$ and H/MT vs. $1/T$ should be linear. According to $M(H)$ in Fig. 2(a), numerical interpolations on H (in 1 emu/g step) are carried out. Figure 3(a) presents the plots of H/T vs. $1/T$ for isometric M up to 50 emu/g (in 5 emu/g step), $H_{\rm exch}$ is obtained by linear fitting of H/T vs. $1/T$. Obviously, the lines with different M are parallel, indicating that the value of λ is weakly dependent on M and T. The $H_{\rm exch}$ is fitted according to $H_{\rm exch} = \lambda_1 M + \lambda_3 M^3$ and the fittings give $\lambda_3 \approx 0$, indicating that the $H_{\rm exch}$ linearly depends on M.[38] Figure 3(b) illustrates the plot of M vs. $(H + H_{\rm exch})/T$ based on $M(H)$. Obviously, almost all the data lie in the same curve which is corresponding to the mean-field state function, indicating reliable fittings. From an odd polynomial fitting of M, the function f is obtained in Fig. 3(b). During this fitting, only those points with higher H are used. In Fig. 3(c), the calculated and experimental $M(H)$ data are compared. Obviously, the calculated results match well with the experimental data except for the magnetic domain regime at the lower magnetic field. From Eq. (5) and using the classical thermo-dynamical theory and Maxwell's relation,[39] $-\Delta S_{\rm M}$ induced by the variation from H_1 to H_2 is given as follows:[31]

$$\begin{aligned}\Delta S_{\rm M}(T)_{\Delta H} &= \int_{H_1}^{H_2} \left(\frac{\partial M}{\partial T}\right)_H {\rm d}H \\ &= \int_{{\rm M}|_{\rm H_1}}^{M|_{H_2}} \left[f^{-1}(M) - \left(\frac{\partial \lambda}{\partial T}\right)_{\rm M} M\right] {\rm d}M. \quad (6)\end{aligned}$$

Generally, the first part of the integral is larger than the second one and the contribution from the second part is smaller. Thus the integral is transformed into an integration of f function. In Fig. 3(d), $-\Delta S_{\rm M}$ is calculated for Mn_3GaC by Eq. (6) and compared with numerical integration of a Maxwell relation. It is found that both the results are in good agreement with each other. Therefore, it is concluded that the mean-field theory can well account for the entropy changes of this system.[40,41]

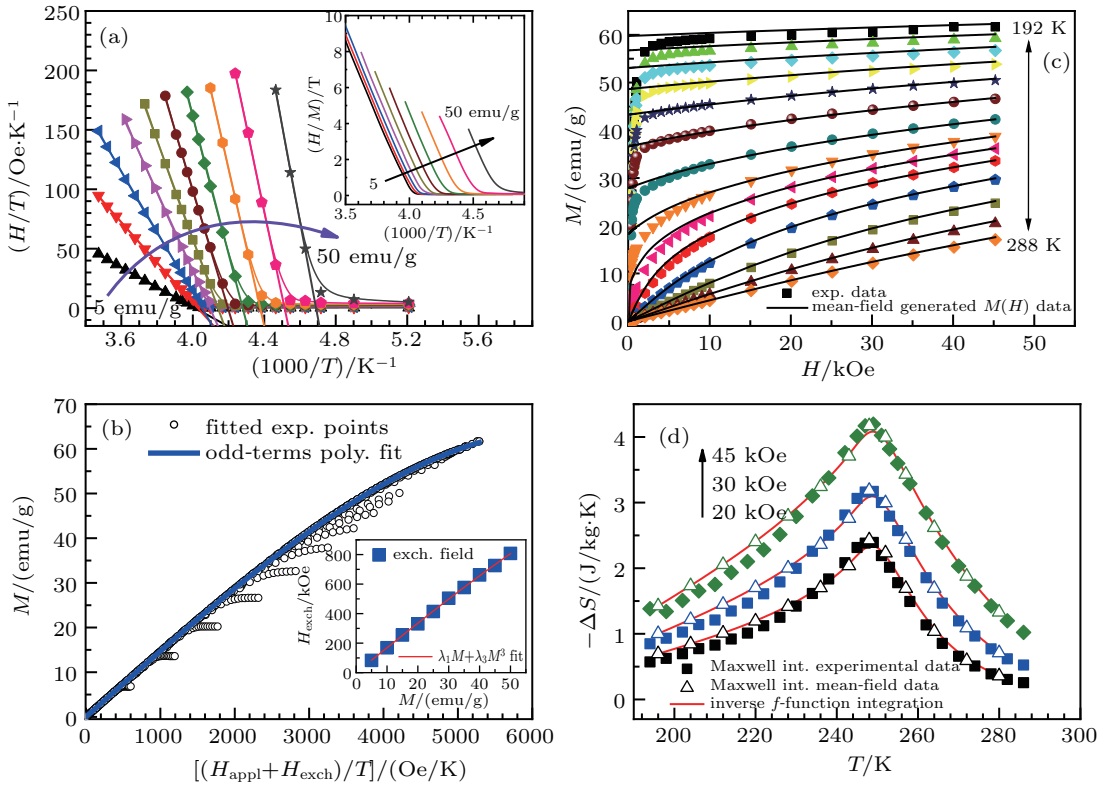

Fig. 3. (a) H/T vs. $1/T$ with constant M. Inset: the plots of H/MT vs. $1/T$. (b) Scaled data in M vs. $(H + H_{\rm exch})$ and polynomial fit. Inset: the exchange field $H_{\rm exch}$ vs. M with the formula $H_{\rm exch} = \lambda_1 M + \lambda_3 M^3$. (c) The experimental and the calculated curves. (d) $\Delta S_{\rm M}$ with $\Delta H = 20$ kOe, 30 kOe, and 45 kOe for comparison.

3.4. The MCE — heat capacity measurement

Another method used to estimate entropy change is based on heat capacity.[42,43] In inset of Fig. 4, the $C_{\rm p}$ vs. T is plotted under $H = 0$ Oe and 20 kOe. A broad peak can be found nearly at 250 K, corresponding to the FM–PM transition. Meanwhile, the peak broadens with increasing the magnetic field. All these characteristics are consistent with the above results. Magnetic entropy change can be $\Delta S(T)_{\Delta H=|H_2-H_1|} = \int_0^T (C(T)_{H_2} - C(T)_{H_1}){\rm d}T/T$ from the second thermodynamics law.[42,43] As shown in Fig. 4, temperature-dependent entropy change $-\Delta S_{\rm M}$ curves for $\Delta H = 20$ kOe with three different methods are compared. It is found that the value of the $-\Delta S_{\rm M}$ exhibits the temperature dependence similar to those of magnetic measurements and the calculations based on the mean-field model except for some differences in details.

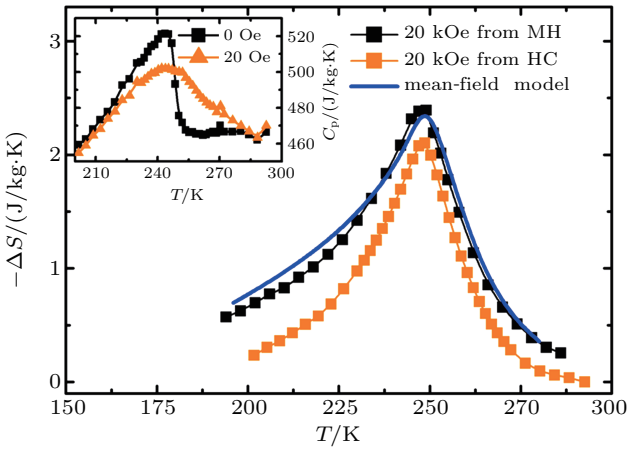

Fig. 4. ΔS_M near the FM–PM phase transition. Inset: heat capacity under $H = 0$ and 20 kOe.

3.5. Direct-current magnetization-critical behavior

According to the scaling hypothesis, a second-order transition near T_c is characterized by critical exponents β (spontaneous magnetization), γ (initial magnetic susceptibility), and δ (critical magnetization isotherm) as follows:[44,45]

$$M_S(T) = M_0|\varepsilon|^{-\beta}, \quad \varepsilon < 0,\ T < T_c, \tag{7}$$

$$\chi_0^{-1}(T) = (h/M_0)\varepsilon^{\gamma}, \quad \varepsilon > 0,\ T > T_c, \tag{8}$$

$$M = DH^{1/\delta}, \quad \varepsilon = 0,\ T = T_c, \tag{9}$$

$\varepsilon = (T - T_c)/T_c$ is the reduced temperature, M_0, h/M_0, and D are the critical amplitudes. Figure 5(a) shows $M(H)$ with $T_c \pm 22$ K. The FM behavior near T_c is investigated by Arrott plots which cover 228–272 K with positive intercepts.[43,46] According to the mean-field theory, M^2 vs. H/M should be parallel lines and the line at $T = T_c$ passes through the origin. In this work, the curves of Arrott plots are flexural, β and γ could not be obtained from $M(H)$ directly. From the Arrott plots in Fig. 5(b), the curves above $T > T_c$ can be extended smoothly into the H/M axis, yielding the $1/\chi_0(T)$. The polynomial fitting and extrapolation for $T < T_c$ give the reliable $M_S(T,0)$. For this extrapolation, M^2 vs. H/M is fitted with a fourth-order polynomial from 4 kOe to 45 kOe, then extrapolated to $H = 0$ to obtain $M_S(T,0)$.[21,22,27]

$M_S(T,0)$ vs. T and $1/\chi_0(T)$ vs. T are given in Fig. 6(a). They denote the power law fitting of $M_S(T,0)$ vs. T and $1/\chi_0(T)$ vs. T according to Eqs. (7) and (8), respectively. For $x = 0$, $\beta = 0.462 \pm 0.02$ with $T_c = 247.29 \pm 0.11$ K and $\gamma = 1.096 \pm 0.01$ with $T_c = 247.91 \pm 0.17$ K. For $x = 0.06$, $\beta = 0.556 \pm 0.03$ with $T_c = 284.52 \pm 0.04$ K and $\gamma = 1.068 \pm 0.02$ with $T_c = 284.87 \pm 0.20$ K. For $x = 0.07$, $\beta = 0.578 \pm 0.01$ with $T_c = 296.74 \pm 0.13$ K and $\gamma = 1.099 \pm 0.04$ with $T_c = 297.16 \pm 0.20$ K. For $x = 0.08$, $\beta = 0.657 \pm 0.01$ with $T_c = 328.26 \pm 0.15$ K and $\gamma = 1.122 \pm 0.03$ with $T_c = 328.70 \pm 0.26$ K. T_c shifts to high temperature with the increase of x. $M_S(T,0)$ and $1/\chi_0(T)$ decreases, and reaches the maximum at $x = 0$. Here β keeps increasing as x increases but γ starts to decrease and then increases.

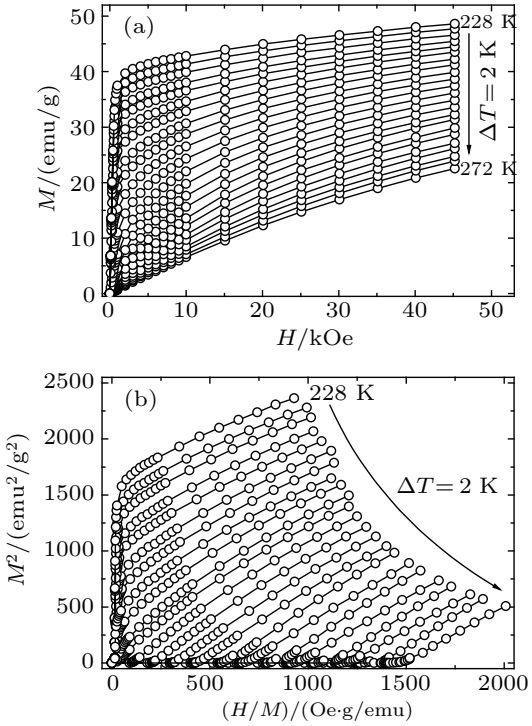

Fig. 5. (a) Isothermal $M(H)$ curves from 228 K to 272 K (in 2 K step). (b) Arrott plots of H/M vs. M^2 derived from $M(H)$ curves.

The exponents are obtained by the Kouvel–Fisher (KF) method,[26,47]

$$M_S(T)[\mathrm{d}M_S(T)/\mathrm{d}T]^{-1} = (T - T_c)/\beta, \tag{10}$$

$$\chi_0^{-1}(T)[\mathrm{d}\chi_0^{-1}(T)/\mathrm{d}T]^{-1} = (T - T_c)/\gamma, \tag{11}$$

$M_S(T)[\mathrm{d}M_S(T)/\mathrm{d}T]^{-1}$ and $\chi_0^{-1}(T)[\mathrm{d}\chi_0^{-1}(T)/\mathrm{d}T]^{-1}$ yield the straight lines with slopes of $1/\beta$ and $1/\gamma$, respectively, and the intercept on the T axis is equal to the value of T_c. For $x = 0$, $\beta = 0.460 \pm 0.004$ with $T_c = 247.56 \pm 0.09$ K and $\gamma = 1.103 \pm 0.005$ with $T_c = 247.69 \pm 0.07$ K. For $x = 0.06$, $\beta = 0.561 \pm 0.003$ with $T_c = 284.54 \pm 0.06$ K and $\gamma = 1.061 \pm 0.05$ with $T_c = 284.94 \pm 0.06$ K. For $x = 0.07$, $\beta = 0.579 \pm 0.001$ with $T_c = 296.74 \pm 0.02$ K and $\gamma = 1.091 \pm 0.007$ with $T_c = 297.27 \pm 0.08$ K. For $x = 0.08$, $\beta = 0.663 \pm 0.001$ with $T_c = 328.60 \pm 0.05$ K and $\gamma = 1.128 \pm 0.01$ with $T_c = 328.65 \pm 0.10$ K. The β keeps increasing as x increases but γ starts to decrease and then increases at $x = 0.07$. The value of $M_S(T)[\mathrm{d}M_S(T)/\mathrm{d}T]^{-1}$ reaches the maximum nearly 55 K at $x = 0.06$ while $\chi_0^{-1}(T)[\mathrm{d}\chi_0^{-1}(T)/\mathrm{d}T]^{-1}$ with the maximum 22.5 K at $x = 0.0$. As shown in Fig. 8, the critical isotherms M vs. H can be correlated by Eq. (9). The reliable fittings are 3.133 ± 0.05 K, 2.950 ± 0.06 K, 2.988 ± 0.05 K, 2.893 ± 0.05 K, respectively. The exponents derived from the scaling analysis are related by the Widom relations.[48,49] We have $\delta = 1 + \gamma/\beta$ from the KF method, δ is close to the value from critical isotherms at T_c, implying that β and γ are reliable.

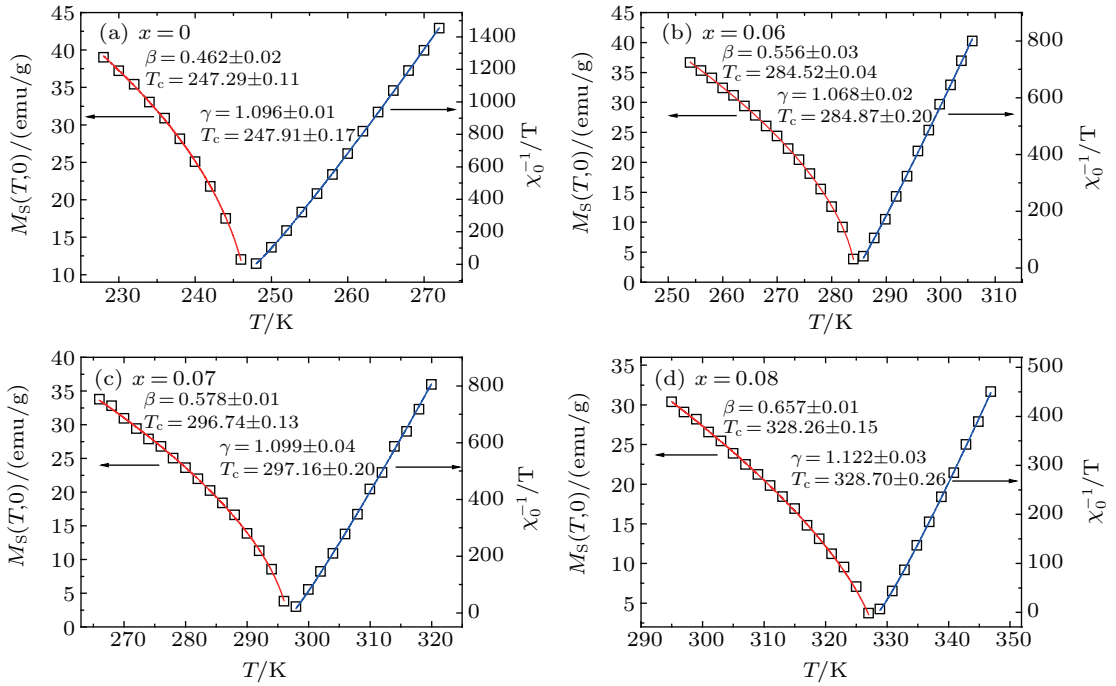

Fig. 6. Temperature dependence of the spontaneous magnetization $M_S(T,0)$ and the inverse initial susceptibility $1/\chi_0(T)$ for $Mn_{3+x}Ga_{1-x}C$.

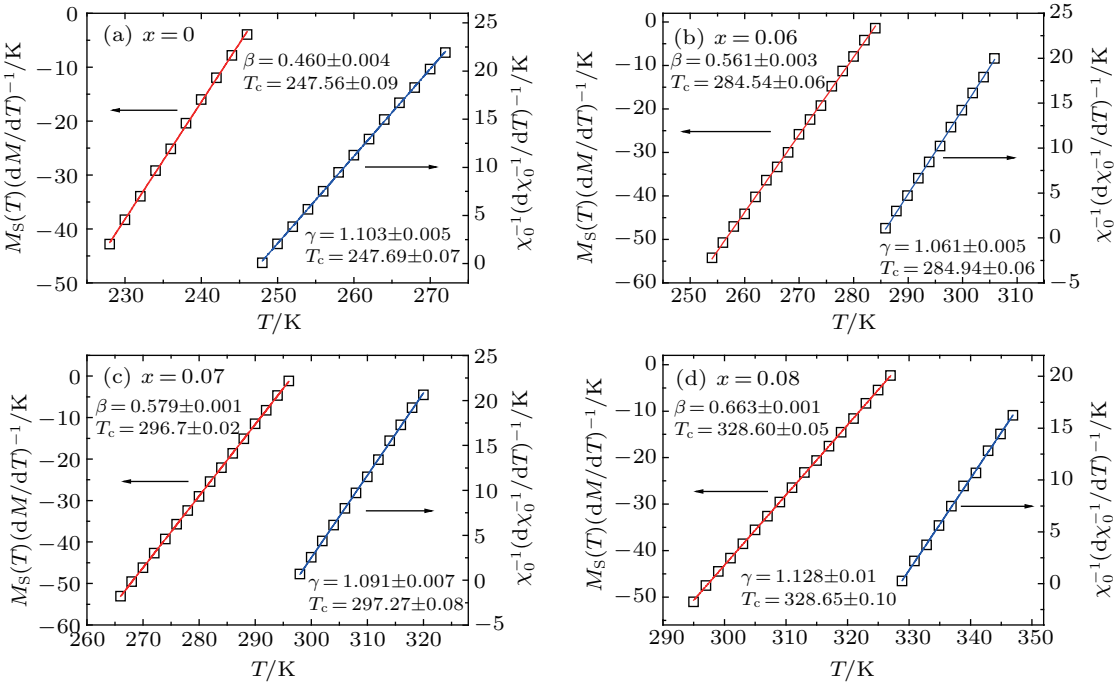

Fig. 7. The Kouvel–Fisher plots for the $M_S(T,0)$ and $1/\chi_0(T)$.

In the critical region, magnetic equation of state is given by[50]

$$M(H,\varepsilon) = |\varepsilon|^{\beta} f_{\pm}(H/|\varepsilon|^{\beta+\gamma}), \tag{12}$$

where f_+ for $T > T_c$ and f_- for $T < T_c$ are regular analytical functions. Equation (12) implies that the plot of $M|\varepsilon|^{-\beta}$ and $H|\varepsilon|^{-(\beta+\gamma)}$ produces two universal curves: one for temperatures below T_c and the other for temperatures above T_c. All the data points lie in two curves, one for $T < T_c$ and the other for $T > T_c$, indicating that exponents and T_c are reliable. In Fig. 9, the plots are shown in log–log scale. We can find that the $M|\varepsilon|^{-\beta}$ increases with the Mn-doping content and the field increases sharply at lower magnetic fields, and flattens out at higher magnetic fields. Obviously, the scaling is reliable, β, γ and δ are close to those of the mean-field model, indicating the appearance of long-range FM interaction in this system. We also find that both the values of β and γ increase with increasing the Mn-doping and are slightly larger than those of

the theoretical model. For clarify, the effective exponents $\beta_{\rm eff}$ and $\gamma_{\rm eff}$ are compared in Fig. 10.[50] Here we define the normalized $\varepsilon = (T - T_{\rm c})/T_{\rm c}$ to be the reduced temperature. It is noticed that the value of $\beta_{\rm eff}$ increases from 0.460 to 0.663 monotonously with the increase of the Mn-doping, while the $\gamma_{\rm eff}$ value decreases from 1.103 for $x = 0$ to 1.061 for $x = 0.06$ firstly and increases again at $x = 0.07$.

By comparison, we can find that critical exponents of this system are apart from those of theoretical models, e.g., 3D Heisenberg and/or 3D Ising models, and mean-field theory.[44,51,52] However, both the values of β

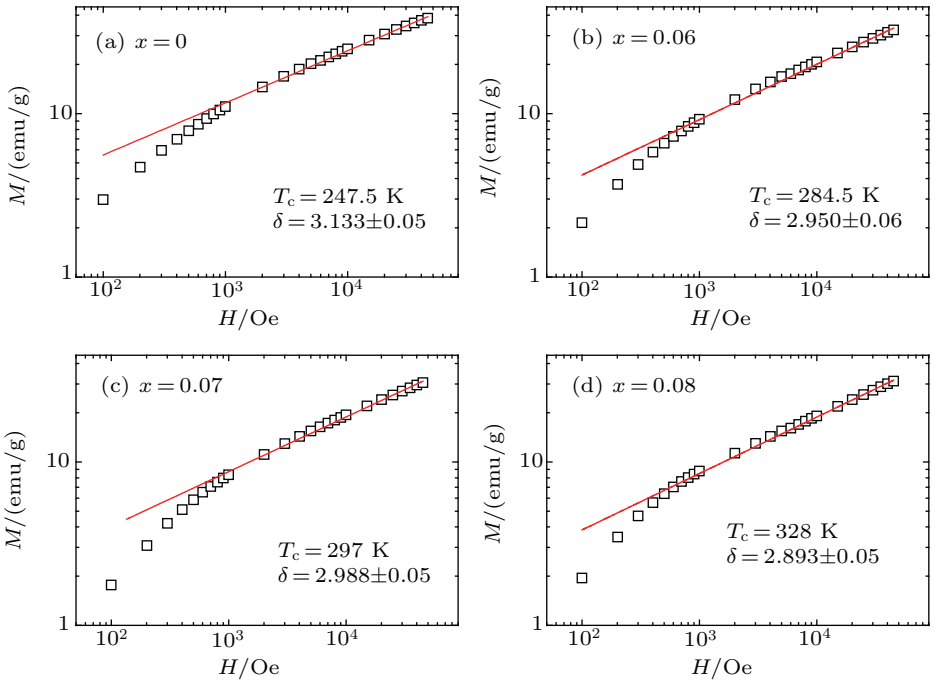

Fig. 8. Critical isotherms on log–log scale for $Mn_{3+x}Ga_{1-x}C$.

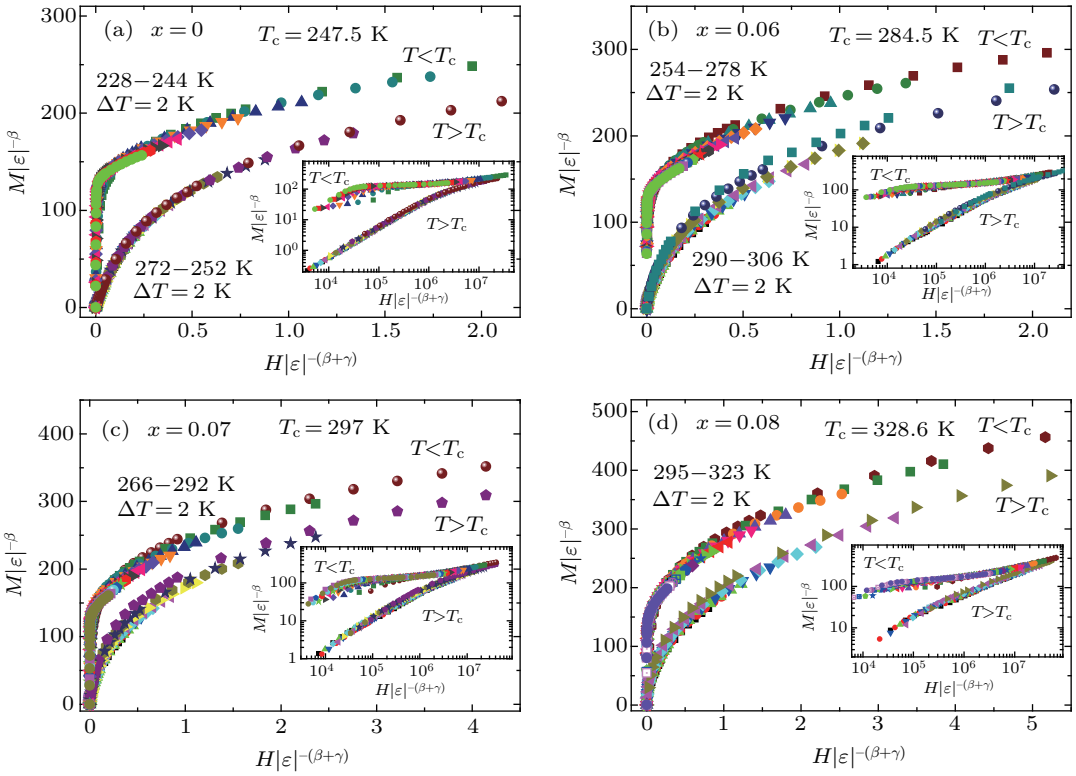

Fig. 9. Scaling plots for $Mn_{3+x}Ga_{1-x}C$ below and above $T_{\rm c}$ using β and γ determined by the Kouvel–Fisher method. The inset shows the plots on a log–log scale.

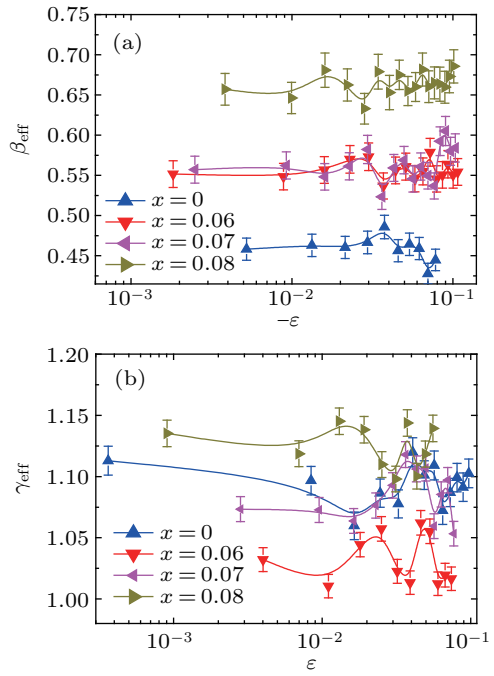

Fig. 10. The dependence of the critical exponent $\beta_{\rm eff}$ and $\gamma_{\rm eff}$ on ε for $Mn_{3+x}Ga_{1-x}C$, where $\varepsilon = (T - T_{\rm c})/T_{\rm c}$ is the reduced temperature.

and γ from the magnetic measurements are just between the predicted mean-field model and the 3D Heisenberg model, and somewhat close to the mean-field model. Usually, the 3D Heisenberg model and the Ising model represent short-range FM interaction and the mean-field model is corresponding to long-range FM coupling.[44,51] Thus, it may be thought that FM interaction is dominant and mainly comes from long-range Mn–C–Mn. Generally, critical exponents depend on lattice dimension, order parameter and the range of interaction (short range, long range or infinite).[53] For magnets, the universality class of transition depends on the exchange interaction $J(r) = 1/r^{d+\sigma}$, where d represents the spatial dimensions and σ is range of interaction and a positive constant.[53] For 3D materials ($d = 3$), there is a relation $J(r) = r^{-(3+\sigma)}$. When $\sigma = 2$, the Heisenberg model is valid for a 3D isotropic ferromagnet, where $J(r)$ decreases faster than r^{-5}. When $\sigma = 3/2$, the mean-field model is satisfied, which indicates that $J(r)$ decreases slower than $r^{-4.5}$. In this work, $\sigma = 1.681 \pm 0.005$ for $x = 0$, $\sigma = 1.634 \pm 0.002$ for $x = 0.06$, $\sigma = 1.671 \pm 0.006$ for $x = 0.07$, $\sigma = 1.714 \pm 0.004$ for $x = 0.08$, implying that $J(r)$ changes from $r^{-4.68}$, $r^{-4.63}$, $r^{-4.67}$, $r^{-4.71}$ for $x = 0$, 0.06, 0.07, 0.08, respectively. It indicates that $J(r)$ of $Mn_{3+x}Ga_{1-x}C$ is close to the mean-field model ($r^{-4.5}$) and trends to the Heisenberg model (r^{-5}) with increasing the Mn-doping. This means that Mn–Mn FM interaction is dominant and the enhanced Mn–C–Mn hybridization derives short-range FM interaction with increasing the Mn doping. Some short-range FM interactions become stronger. The detailed mechanism requires more investigations.

4. Conclusions

MCE near FM–PM transition in Mn_3GaC has been investigated. Molecular mean-field model can well describe $-\Delta S_{\rm M}$, while the Landau theory model does not. In addition, critical behavior is investigated by magnetization measurements using three different techniques. Critical exponents of Mn-rich Mn_3GaC are between the mean-field model and the Heisenberg model. Mn–Mn FM interaction is dominant and the enhanced Mn–C–Mn hybridization derives short-range FM interaction with increasing the Mn doping.

Acknowledgments

We thank Professor P. Tong, Professor Y. P. Sun, Professor J. G. Cheng for useful assistance.

References

[1] Kamishima K, Goto T, Nakagawa H, *et al.* 2000 *Phys. Rev. B* **63** 024426
[2] Wang B S, Tong P, Sun Y P, Li L J, Tang W, Lu W J, Zhu X B, Yang Z R and Song W H 2009 *Appl. Phys. Lett.* **95** 222509
[3] Tohei T, Wada H and Kanomata T 2003 *J. Appl. Phys.* **94** 1800
[4] Yu M H, Lewis L H and Moodenbaugh A R 2003 *J. Appl. Phys.* **93** 10128
[5] Tohei T, Wada H and Kanomata T 2004 *J. Magn. Magn. Mater.* **272** E585
[6] Wang B S, Tong P, Sun Y P, Luo X, Zhu X B, Zhang S B, Zhu X D, Yang Z R, Dai J M and Song W H 2009 *Europhys. Lett.* **85** 47004
[7] Takenaka K, Asano K, Misawa M and Takagi H 2008 *Appl. Phys. Lett.* **92** 011927
[8] Tong P, Louca D, Kingdom G, Liobet A, Lin J C and Sun Y P 2013 *Appl. Phys. Lett.* **102** 041908
[9] Iikubo S, Kodama K, Takenaka K, *et al.* 2008 *Phys. Rev. Lett.* **101** 205901
[10] Takenaka K and Takagi H 2009 *Appl. Phys. Lett.* **94** 131904
[11] J Huang R, Li L F, Cai F S, Xu X D and Qian L H 2008 *Appl. Phys. Lett.* **93** 081902
[12] Ding L, Wang C, Sun Y, Colin C V and Chu L H 2015 *J. Appl. Phys.* **117** 213915
[13] Guo X G, Lin J C, Tong P, Wang M, Wu Y, Yang C, Song B, Lin S, Song W H and Sun Y P 2015 *Appl. Phys. Lett.* **107** 202406
[14] Shimizu T, Shibayama T, Asano K and Takenaka 2012 *J. Appl. Phys.* **111** 07A903
[15] Guo X G, Tong P, Lin J C, Yang C, Zhang K, Lin S, Song W H and Sun Y P 2017 *Appl. Phys. Lett.* **110** 062405
[16] Asano K, Koyama K and Takenaka K 2008 *Appl. Phys. Lett.* **92** 161909
[17] Kim W S, Chi E O, *et al.* 2001 *Solid State Commun.* **119** 507
[18] Shim J H, Kwon S K and Min B I 2002 *Phys. Rev. B* **66** 020406(R)
[19] Fruchart D, Bertaut E F, Sayetat F, *et al.* 1970 *Solid State Commun.* **8** 91
[20] Wang B S, Tong P, Sun Y P, Zhu X B, Luo X, Li G, Song W H, Yang Z Rand Dai J M 2009 *J. Appl. Phys.* **105** 083907
[21] Cabassi R, Bolzoni F, Gauzzi A and Licci F 2006 *Phys. Rev. B* **74** 184425
[22] Yang J, Lee Y P and Li Y 2007 *Phys. Rev. B* **76** 054442
[23] Lin J C, Tong P, Cui D P, Yang C, Yang J, Lin S, Wang B S, Tong W, Zhang L, Zou Y M and Sun Y P 2015 *Scr. Rep.* **5** 7933
[24] Cui D P, Wang B S, Tong P, Lin J C, Lin S and Sun Y P 2015 *J. Magn. Magn. Mater.* **382** 93
[25] Zhang L, Wang B S, Sun Y P, Tong P, Fan J Y, Zhang C J, Pi L and Zhang Y H 2012 *Phys. Rev. B* **85** 104419
[26] Babu P D and Kaul S N 1997 *J. Phys.: Condens. Matter* **9** 7189
[27] Pramanik A K and Banerjee A 2009 *Phys. Rev. B* **79** 214426
[28] Yang J, Lee Y P and Li Y 2007 *J. Appl. Phys.* **102** 033913
[29] Amaral V S and Amaral J S 2004 *J. Magn. Magn. Mater.* **272–276** 2104
[30] Lu W J, Luo X, Hao C Y, Song W H and Sun Y P 2008 *J. Appl. Phys.* **104** 113908
[31] Amaral J S, Silva N J O and Amaral V S 2007 *Appl. Phys. Lett.* **91** 172503

[32] Amaral J S and Amaral V S 2009 *Appl. Phys. Lett.* **94** 042506
[33] Banerjee S K 1964 *Phys. Lett.* **12** 16
[34] Landau L D and Lifshitz E M 1980 *Statistical Physica* 3rd Edn. (Oxford: Pergamon)
[35] Amaral J S, Reis M S, *et al.* 2005 *J. Magn. Magn. Mater.* **290–291** 686
[36] Yang J, Sun Y P, Song W H and Lee Y P 2006 *J. Appl. Phys.* **100** 123701
[37] Bean C P and Rodbell D S 1962 *Phys. Rev.* **126** 104
[38] Menyuk N, Dwight K and Reed T B 1971 *Phys. Rev. B* **3** 1689
[39] Gschneidner K A and Pecharsky V K 2000 *Annu. Rev. Mater. Sci.* **30** 387
[40] Yang F Y, Chien C L, Li X W, Xiao G and Gupta A 2001 *Phys. Rev. B* **63** 092403
[41] Yanagihara H, Cheong W, *et al.* 2002 *Phys. Rev. B* **65** 092411
[42] Gschneidner Jr. K A, Pecharsky V K and Tsokol A O 2005 *Rep. Prog. Phys.* **68** 1479
[43] Tishin A M and Spichkin Y I 2003 *The Magnetocaloric Effect and its Applications* (Bristol: Institute of Physics Publishing)
[44] Stanley H E 1972 *Introduction to Phase Transitions and Critical Phenomena* (Oxford: Clarendon Press)
[45] Fisher M E 1967 *Rep. Prog. Phys.* **30** 615
[46] Mira J, Rivas J, *et al.* 1999 *Phys. Rev. B* **60** 2998
[47] Kouvel J S and Fisher M E 1964 *Phys. Rev.* **136** A1626
[48] Widom B 1964 *J. Chem. Phys.* **41** 1633
[49] Widom B 1965 *J. Chem. Phys.* **43** 3898
[50] Stanley H E 1999 *Rev. Mod. Phys.* **71** S358
[51] Huang K 1987 *Statistical Mechanics* 2nd Edn. (New York: Wiley)
[52] Le J C and Zinn-Justin J 1980 *Phys. Rev. B* **21** 3976
[53] Fisher M E, Ma S K and Nickel B G 1972 *Phys. Rev. Lett.* **29** 917